Journal of Colloid and Interface Science 448 (2015) 451–459

Contents lists available at ScienceDirect

Journal of Colloid and Interface Science

www.elsevier.com/locate/jcis

# Highly effective adsorption of cationic and anionic dyes on magnetic Fe/Ni nanoparticles doped bimodal mesoporous carbon

Yuanyuan Liu, Guangming Zeng *, Lin Tang *, Ye Cai, Ya Pang, Yi Zhang, Guide Yang, Yaoyu Zhou, Xiaoxiao He, Yan He

*College of Environmental Science and Engineering, Hunan University, Changsha 410082, Hunan, PR China*
*Key Laboratory of Environmental Biology and Pollution Control (Hunan University), Ministry of Education, Changsha 410082, Hunan, PR China*

## GRAPHICAL ABSTRACT

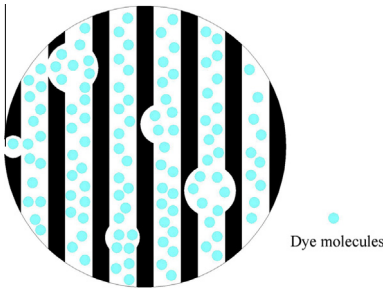


## ARTICLE INFO

*Article history:*
Received 9 October 2014
Accepted 12 February 2015
Available online 26 February 2015

*Keywords:*
Fe/Ni nanoparticles
Magnetic bimodal mesoporous carbon
Adsorption
Cationic dyes
Anionic dyes

## ABSTRACT

Magnetic Fe/Ni nanoparticles doped bimodal mesoporous carbon (MBMC) was prepared for highly effective adsorption of cationic dye methylene blue (MB) and anionic dye methyl orange (MO). Structure characterization demonstrated that Fe/Ni nanoparticles were embedded into the interior of the mesoprous carbon, and MBMC maintained ordered and bimodal mesopores. The effects of several parameters such as contact time, pH, temperature, ionic strength and dye molecular structure on the adsorption were investigated. Alkaline pH was better for MB adsorption, while acidic pH was more favorable for MO uptake. The adsorption capacity was slightly enhanced when existing ion concentrations increased. Adsorption on MBMC was affected by the molecular structures of different dyes, and both primary and secondary pores of MBMC were involved in dye adsorption. The adsorption kinetics fitted well with pseudo-second-order model and exhibited 3-stage intraparticle diffusion mode. Equilibrium data were best described by Langmuir model, and the estimated maximum adsorption capacity for MB and MO was 959.5 mg/g and 849.3 mg/g, respectively. Thermodynamic studies indicated that the adsorption process was spontaneous and endothermic. Moreover, the adsorbent could be regenerated using ethanol, and the regenerated adsorbent after seven cycles could retain over 80% of the adsorption capacity for the fresh adsorbent. The results suggested that MBMC could be considered as very effective and promising materials for both anionic and cationic dyes removal from wastewater.



## 1. Introduction

Water pollution during the rapid industrialization has become a major issue worldwide [1,2]. Among the numerous aqueous

* Corresponding authors at: College of Environmental Science and Engineering, Hunan University, Changsha 410082, Hunan, PR China. Fax: +86 731 88823701.
*E-mail addresses:* zgming@hnu.edu.cn (G. Zeng), tanglin@hnu.edu.cn (L. Tang).

http://dx.doi.org/10.1016/j.jcis.2015.02.037
0021-9797/

pollutants, dyes have aroused increasing public concerns due to their extensive use in many industries, such as textile, pharmaceutical, printing, leather and food industry [3,4]. The discharge of dye wastewater interferes with the photosynthetic activities of the aquatic life; moreover, a large number of dyes and their metabolites have been reported to be toxic and carcinogenic [3,5]. However, the poor degradable nature toward light and oxidizing agents of dyes make them difficult to be removed by traditional techniques [6]. Therefore, various techniques, including coagulation, filtration, oxidation, membrane separation, biodegradation and adsorption, have been developed for dye effluent treatment [6–8].

Among all the techniques for wastewater treatment, adsorption has been recognized as one of the most straightforward, convenient and effective method for the removal of a variety of pollutants [9,10]. The key to adsorption technology lies in the effectiveness and efficiency of adsorbent. Although commercial activated carbon has been most widely applied in adsorption, its microporous nature has limited the pore utility and adsorption capacity for large molecules [6]. Limited adsorption for bulky molecules is also found in another commonly used adsorbent, zeolite, which comprises an aluminosilicate cage-like micro-structure [11]. As an alternative to the microporosity of the activated carbons and zeolites, ordered mesoporous carbon materials, with their unique properties such as regular mesoporous structure, high specific surface area and large pore volume, have been reported to be advantageous for the adsorption of a large variety of sorbates, especially for large molecules such as dyes [11,12]. Moreover, with their higher hydrothermal stability, mesoporous carbon materials could be more resistant to harsh environments, thus could be more widely used [13].

Compared with conventional separation techniques such as filtration, centrifugation and precipitation, magnetic separation technology is a promising technique with its easy operation and fast separation [14]. Therefore, introducing Fe-, Ni- and Co-containing nanoparticles into mesoporous materials have been extensively studied [5,15]. However, the introduction of magnetic nanoparticles into mesoporous materials might block the pores and resist the mass transfer, reducing adsorption efficiency [16]. Thus, it is essential to develop magnetic nanoparticle-doped mesoporous adsorbents with high adsorption efficiency. Also, high magnetization saturation value is essential for the efficient separation of the adsorbent, and the magnetic strengths of Fe/Ni alloy has been reported to be stronger than the pure Fe or Ni metals [17,18]. Although there have been reports about the magnetic mesoporous carbon as adsorbents, few of them have investigated Fe/Ni doped mesoporous carbon. And it has been reported that mesoporous materials with bimodal mesopores might exhibited higher adsorption capacity than the ones with unimodal pores [19]; however, to the best of our knowledge, there have been no reports for the removal of dyes using Fe/Ni doped bimodal mesoporous carbon.

In this study, a novel adsorbent, with its high saturation magnetization value and unique bimodal mesoporous structure, has been applied in the adsorption of different dyes. Methylene blue (MB) and methyl orange (MO), as a typical cationic and anionic dye, respectively, were selected as the main adsorbates for the present study. Sorption kinetics, isotherms and thermodynamic studies for the adsorption of MB and MO were conducted, and the effects of pH and ionic strength on the adsorption for the two dyes were also tested. To improve the economic use of the adsorbent, the adsorbent was regenerated and the reusability was evaluated. Moreover, to study the adsorption mechanism, the role of secondary pores in adsorption and the effects of dye molecular structure of five different dyes on adsorption were studied.

## 2. Materials and methods

### 2.1. Materials

Pluronic copolymer P123 ($EO_{20}PO_{70}EO_{20}$) (Mav = 5800) were purchased from Sigma–Aldrich (USA). All other chemicals were of analytical grade and were used as received without further purification.

### 2.2. Synthesis of adsorbents

Magnetic Fe/Ni nanoparticle decorated bimodal mesoporous carbon (MBMC) was prepared according to a co-impregnation method with slight alterations [17]. The silica template SBA-15 was prepared according to a method reported [20]. Then, 1.5 mL of a multi-component solution which contains 0.8 mmol $Fe(NO_3)_3{\cdot}9H_2O$, 0.8 mmol $Ni(NO_3)_2{\cdot}6H_2O$, 0.5 mL ethanol and 1 mL furfuryl alcohol was infiltrated into 1.2 g SBA-15 template. The impregnated mixture was cured at 80 °C in air for 10 h, followed by carbonization and in situ reduction of the metal oxides under a mixture of 5% $H_2$–95% Ar at 900 °C for 2 h. The product was washed by heated 2 M NaOH solution and water, dried and stored for future experiments.

### 2.3. Characterization

$N_2$ adsorption–desorption isotherms were measured on a Micromeritics 2020 analyzer at 77 K. The surface area and the total pore volume were calculated based on Brunauer–Emmett–Teller (BET) and Barrett–Joyner–Halenda (BJH) analyses, respectively. And desorption branches of the isotherms were used to derive pore size distribution. The scanning electron images (SEM) were performed using Field Emission scanning electron microscope (FE-SEM, JEOL JSM-6700F). Transmission electron microscopy (TEM) images were taken on a JEOL-1230 electron microscope operated at 100 kV. Zeta Potential was determined by first dispersing MBMC in 1 mmol/L NaCl solution with various pH values by sonication, and then measuring the supernatant with Zetasizer Nano (ZEN3600, Malvern). The magnetic properties of the composites were studied by a vibrating sample magnetometer (VSM) at room temperature.

### 2.4. Batch mode adsorption

To investigate the nature and molecular structure on adsorption, MB, MO and three another commercial dyes, namely brilliant yellow (BY), rhodamine B (RB) and reactive red 2 (RR2) were selected for the adsorption study. The chemical formulas, chemical and structural properties of these dyes were summarized in Table 1. The batch mode adsorption studies for various dyes were

**Table 1**
General chemical properties of each dye.

| Dye | Molecular weight (g/mol) | Molecular size (nm) | Nature | Concentration (mg/L) | $\lambda_{max}$ (nm) |
|---|---|---|---|---|---|
| Methylene blue (MB) | 320 | 1.26 × 0.77 × 0.65 | Cationic | 50–800 | 665 |
| Methyl orange (MO) | 327 | 1.31 × 0.55 × 0.18 | Anionic | 50–800 | 465 |
| Brilliant yellow (BY) | 625 | 2.45 × 1.09 × 0.36 | Anionic | 500 | 400 |
| Rhodamine B (RB) | 478 | 1.59 × 1.18 × 0.56 | Cationic | 500 | 554 |
| Reactive red 2 (RR2) | 617 | 1.9 × 1.7 × 0.5 | Anionic | 500 | 538 |

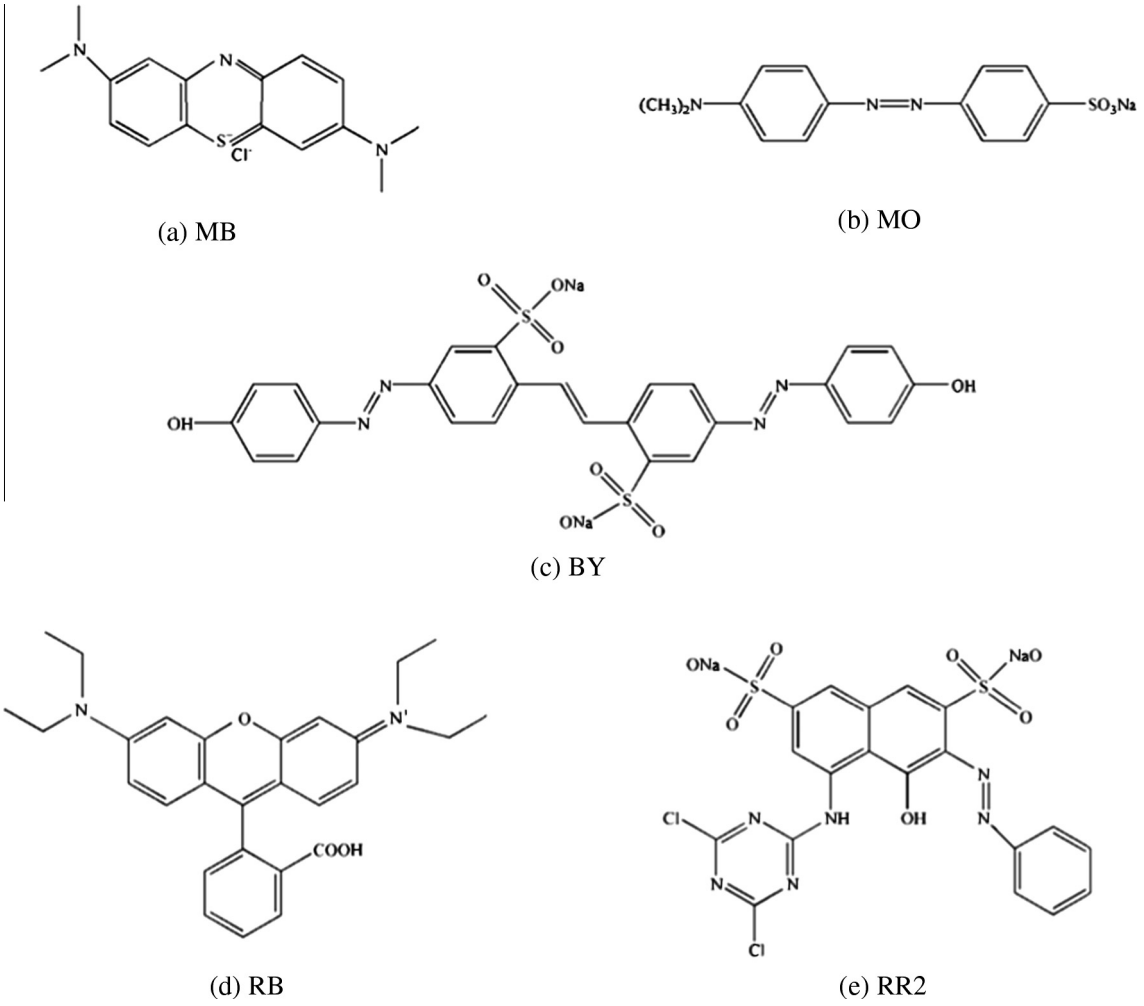


**Fig. 1.** Molecular structure of the studied dyes.

carried out by agitating 5 mg of MBMC in 25 mL of dye solution. The mixture was continuously shaken on a shaker at 150 rpm under controlled temperature of 25 °C until reaching equilibrium. The solution pH was adjusted using HCl or NaOH solutions. After adsorption, the adsorbent was separated from the solution under magnetism, and then the dye concentration in the clear solution was measured at the maximum absorbance of each dye by a UV–vis spectrophotometer.

The adsorption capacity of each dye in the adsorption system, $q_e$, was calculated by

$$q_e = \frac{(C_i - C_e)V}{m} \tag{1}$$

where $C_i$ and $C_e$ are initial and equilibrium concentrations (mg/L), respectively; $m$ is the mass of the adsorbent (g); and $V$ is volume of the solution (L).

Effects of pH and ionic strength on the adsorption performance were investigated with each dye concentration of 150 mg/L and equilibrium time of 2 h. To study the effect of coexisting ions on dye adsorption, Sodium chloride and calcium nitrate solutions from 100 to 1000 mg/L were used in the adsorption system. Each set of experiments was carried out in duplicate, and the arithmetic mean values were calculated, with the standard deviations less than 5%.

### 2.5. Kinetic studies

Sorption kinetic studies were conducted at 25 °C under initial dye concentration of 150 mg/L. Adsorption kinetics were studied using two kinetic models, namely the pseudo-second-order model and the intraparticle diffusion model.

The pseudo-second-order kinetic model is described by the formula

$$\frac{t}{q_t} = \frac{1}{k_{ad}q_e^2} + \frac{1}{q_e}t \tag{2}$$

where $q_e$ and $q_t$ are, respectively, the amount of dyes adsorbed at the equilibrium and time $t$ (mg/g); and $k_{ad}$ is the pseudo-second-order rate constant for the adsorption process (mg/g min).

The intraparticle diffusion model is expressed by the equation

$$q_t = k_{id}t^{0.5} + C \tag{3}$$

where $k_{id}$ stands for the intraparticle diffusion rate constant (mg/g $h^{1/2}$), and $C$ (mg/g) is the constant varied directly with the boundary layer thickness.

### 2.6. Adsorption isotherm and thermodynamic studies

Adsorption isotherms at 25 °C, 35 °C and 45 °C were studied respectively, with MB and MO concentration varying from 50 to

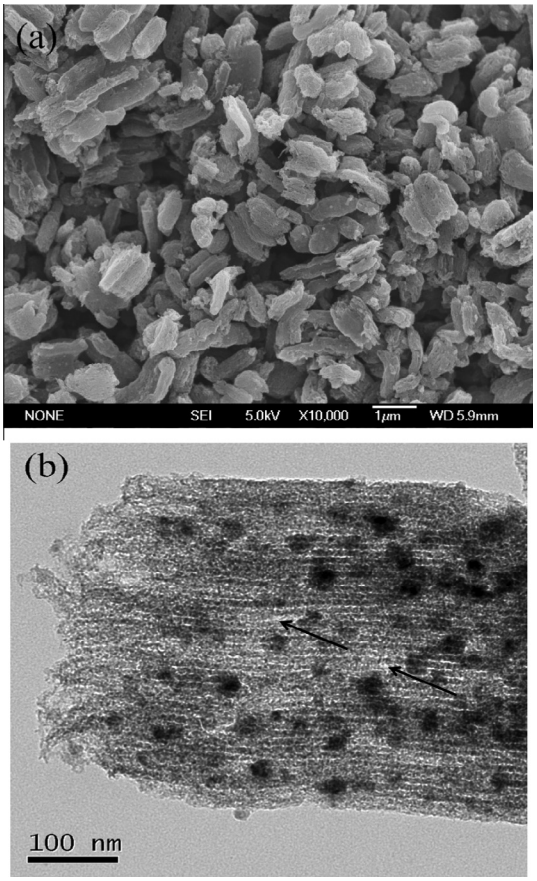


**Fig. 2.** SEM (a) and TEM (b) images of MBMC.

800 mg/L. The equilibrium data were subject to simulate with Langmuir and Freundlich isotherm models.

The Langmuir equation could be described as

$$q_e = \frac{q_m b C_e}{1 + bC_e} \tag{4}$$

where $q_e$ stands for the equilibrium adsorption capacity (mg/g), $C_e$ is the concentration of dyes at equilibrium (mg/L), $q_m$ is the maximum adsorption capacity (mg/g), and $b$ is the equilibrium adsorption constant (L/mg).

Based on the analysis of Langmuir model, the adsorption system could be further evaluated by the dimensionless parameter ($R_L$), which could be defined as

$$R_L = \frac{1}{1 + bC_0} \tag{5}$$

where $C_0$ is the initial concentration of the dyes. According to the value of $R_L$, the adsorption process could be evaluated as irreversible ($R_L = 0$), favorable ($0 < R_L < 1$), linear ($R_L = 1$) and unfavorable ($R_L > 1$).

The Freundlich isotherm model is defined as

$$q_e = K_F C_e^{1/n} \tag{6}$$

where $K_F$ and $n$ are the Freundlich constant and the heterogeneity factor, indicating the adsorption capacity and the adsorption intensity of the adsorbent, respectively.

To study the thermodynamics of MO and MB adsorption on MBMC, the thermodynamic parameters such as Gibbs free energy change ($\Delta G$, kJ/mol), enthalpy change ($\Delta H$, kJ/mol) and entropy change ($\Delta S$, kJ/mol) could be obtained using the equations listed below:

$$\Delta G = -RT \ln b \tag{7}$$

$$\ln b = \frac{\Delta S}{R} - \frac{\Delta H}{RT} \tag{8}$$

where $b$ is the equilibrium adsorption constant (L/mg), $R$ is the ideal gas constant (8.31 J/mol K), and $T$ is the temperature (K).

### 2.7. Desorption and regeneration of adsorbent

The feasibility of desorption and reuse of the adsorbent was evaluated using ethanol. After agitating 5 mg of MBMC with 25 mL of dye solution under optimum conditions, dye loaded adsorbent was washed, dried and added into 25 mL of ethanol for desorption at 150 rpm at 25 °C for 24 h. The adsorbent was magnetically separated, washed and tested for further adsorption of MO and MB under same adsorption condition.

## 3. Results and discussion

### 3.1. Characterization

Fig. 2a shows a typical SEM image of MBMC, and a platelet-like shape with the average size around 0.5 μm could be observed. TEM image (Fig. 2b) is used to directly observe the pore structure of the

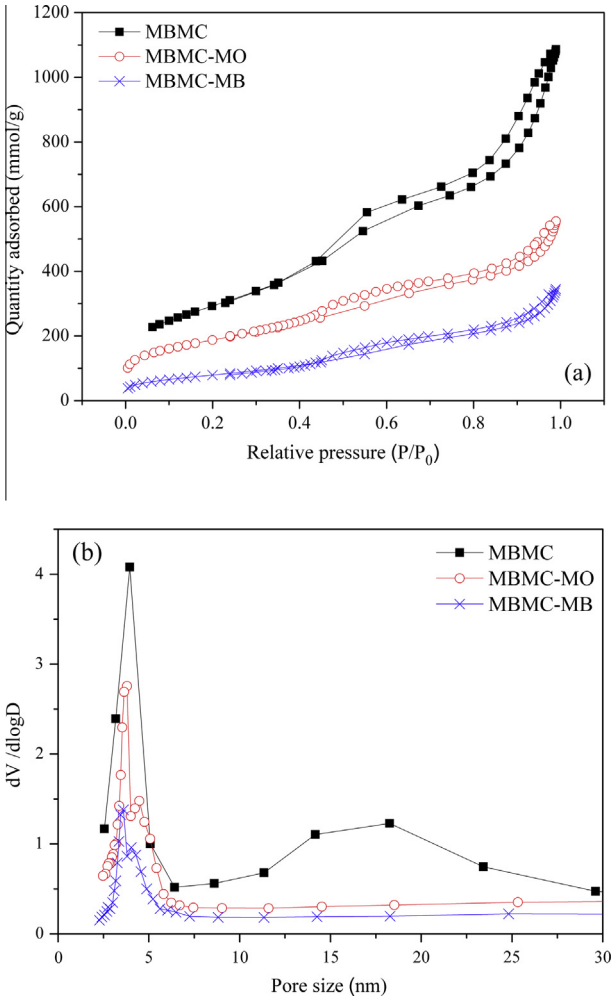


**Fig. 3.** (a) Nitrogen adsorption–desorption isotherms for MBMC before and after adsorption of MB and MO; (b) the corresponding pore size distributions of MBMC before and after adsorption of dyes.

**Table 2**
Pore structure parameters of MBMC before and after dye adsorption.

| Sample[a] | $S_{BET}$ ($m^2$/g) | $S_{BJH}$ ($m^2$/g) | $V_{BJH}$ ($cm^3$/g) | Pore size (nm) |
|---|---|---|---|---|
| MBMC | 1057.9 | 1091.2 | 1.78 | 4.0, 18.5 |
| MBMC–MB | 100.6 | 111.2 | 0.17 | 3.6, 4.0 |
| MBMC–MO | 431.9 | 350.5 | 0.53 | 3.8, 4.5 |

[a] The suffix in the sample name represents the adsorbed dye.

adsorbent, and the ordered stripe-like pores of the adsorbent could be observed, confirming the presence of ordered mesoporous structure. Dark spots representing Fe/Ni nanoparticles were well dispersed into the carbon matrix, while the voids marked by arrows were the secondary pores [21].

MBMC shows type IV isotherm (Fig. 3a), indicating the characteristic of uniform mesopores. The two hysteresis loops of the isotherm indicated the presence of two different pores [22], and the two most probable pore sizes centered at 4.0 nm and 18.5 nm also confirmed the bimodal-like pore size distribution (Fig. 3b). The surface area, pore volume of MBMC based on BET and BJH analyses are listed in Table 2. The magnetization saturation value for MBMC is 12.4 emu/g (Fig. 4); indicating that the separation of MBMC in aqua media could be controlled under magnetic fields. And according to the inset of Fig. 4, MBMC after dye adsorption could be effectively separated from the water using an outer magnet, further demonstrating the magnetic properties of MBMC.

### 3.2. Effect of pH

The removal of MB and MO as a function of pH was studied in the range of pH values from 3.0 to 10.0. As shown in Fig. 5b, the equilibrium adsorption capacity for MB experienced a steady increase from 279.6 mg/g to 371.9 mg/g with the increase of the pH, while the adsorbed amount MO decreased from 298.7 mg/g to 247.7 mg/g. The different effects of pH on MB and MO adsorption could be explained by the electrostatic repulsion [22]. Since the point of zero charge (PZC) of MBMC is around 4 according to the zeta potential results (Fig. 5a), when the pH values of the dye solutions were higher than PZC, the surface of MBMC was negatively charged. And the surface was more negatively charged when the pH increased, which was more favorable for the adsorption of cationic dyes such as MB. On the contrary, the adsorption of MO was reduced due to the weaker electrostatic reaction between the more negatively charged surface of the adsorbent and the anionic dye (MO).

### 3.3. Effect of coexisting ions

Dye effluents always contain a large variety of coexisting ions, which might affect the dye adsorption process [23]. In this study, two commonly coexisting salts, NaCl and $Ca(NO_3)_2$, were selected to study the effect on MB and MO adsorption capacity by MBMC, with the results presented in Fig. 6. The amount of MB and MO adsorbed onto MBMC both experienced a tiny increase with the increasing concentration of NaCl or $Ca(NO_3)_2$. On one hand, the increase in the salt concentration could promote the dissociation of the dye molecules by facilitating protonation, resulting in higher adsorption capacity. On the other hand, increasing ionic strength will decrease the dye uptake when the electrostatic repulsion is not repulsive [24]. The adsorption process was conducted under pH > $pH_{PZC}$, favorable for the electrostatic reaction between cationic dye (MB) and the negatively charged adsorbent. Thus the former effect of the coexisting ions is dominant for MB adsorption. Since the electrostatic force between MO and MBMC is not repulsive, the increased amount of MO was caused by both of the two effects mentioned above, and the increase in MO uptake was slightly more than MB. It is also notable that the effect of $Ca(NO_3)_2$ on the adsorption of both MO and MB is also slightly higher than NaCl, which might be resulted from the more positively charge

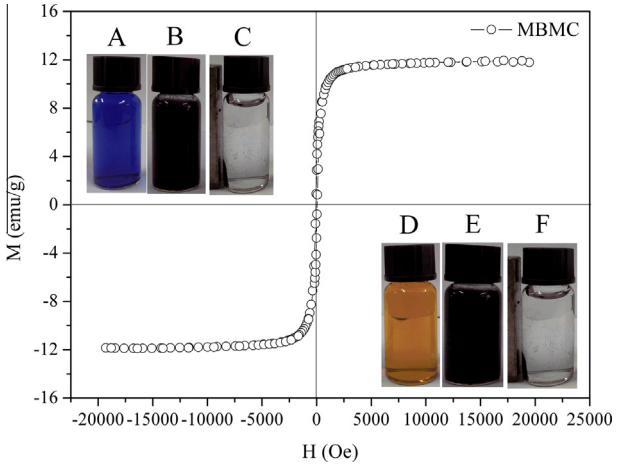


**Fig. 4.** Magnetization curves of MMC. Inset are photographs for dye water solution before (A, D), after adsorption by adding MBMC (B, E) and after being separated using an outer magnet (C, F): (A, B, C) MB, (D, E, F) MO. (adsorbent dosage 20 mg/L, initial dye concentrations 50 mg/L, pH 7.0, contact time 2 h, temperature 25 °C).

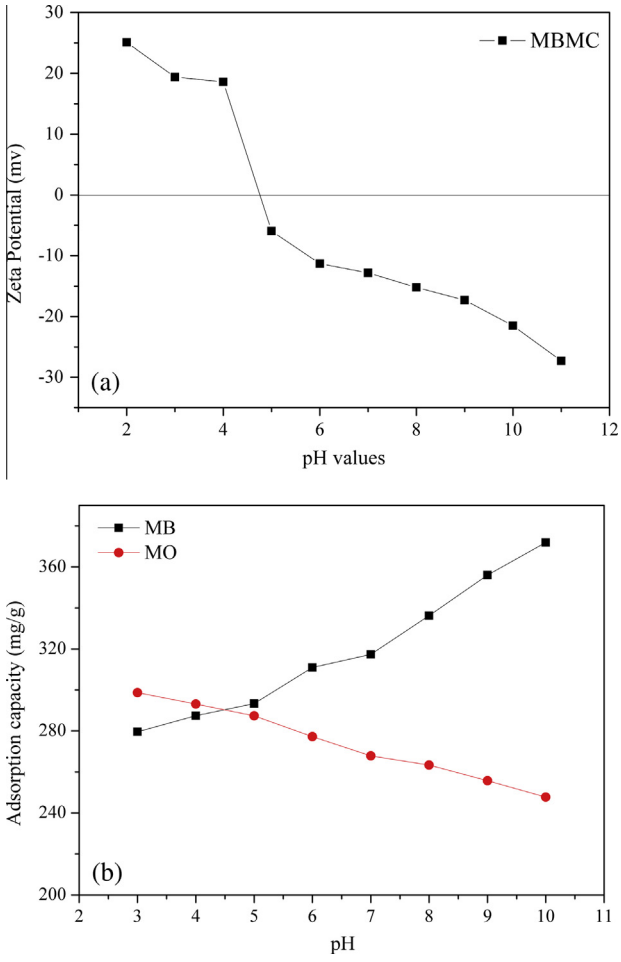


**Fig. 5.** (a) Zeta potential of MBMC as a function of pH; (b) Effect of pH on MB and MO adsorption by MBMC (adsorbent dosage 20 mg/L, initial dye concentrations 150 mg/L, contact time 2 h, temperature 25 °C).

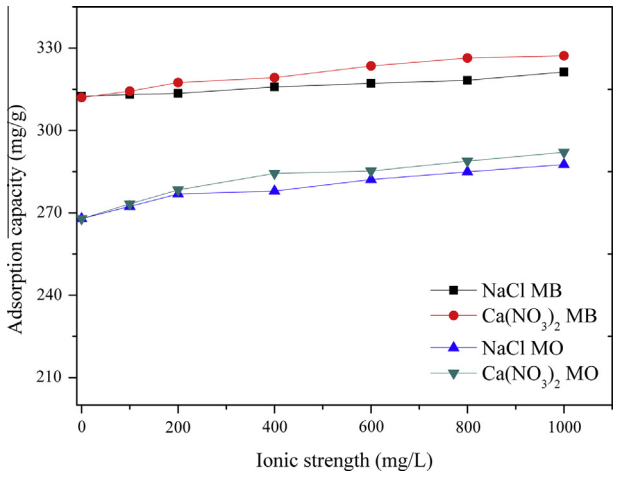


**Fig. 6.** Effect of common salts on MB and MO adsorption capacity by MBMC (adsorbent dosage 20 mg/L, initial dye concentrations 150 mg/L, contact time 2 h, pH 7.0, temperature 25 °C).

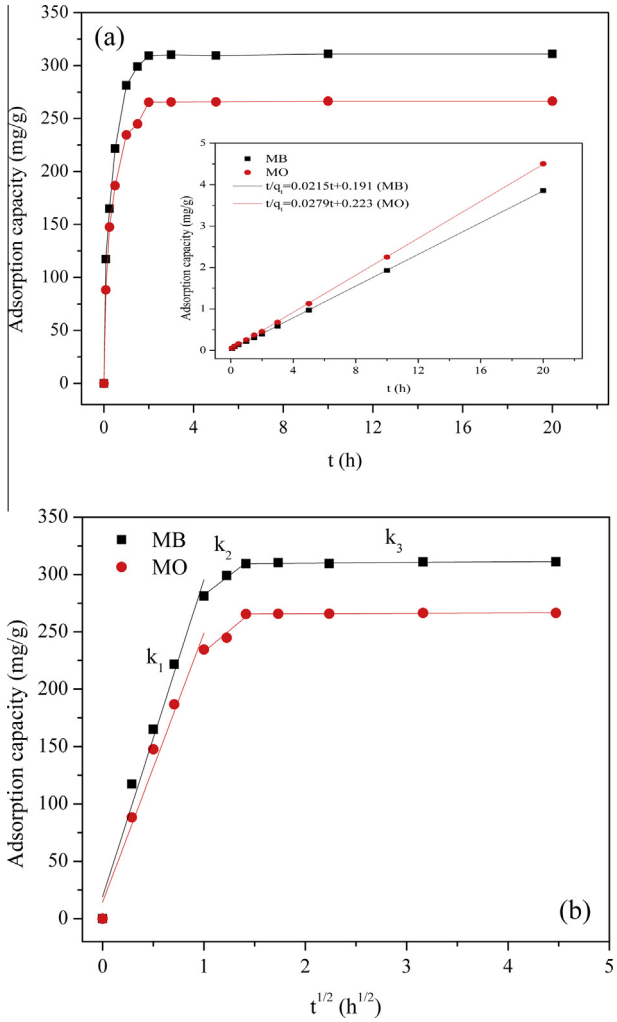


**Fig. 7.** (a) Adsorption kinetics of MB and MO by MBMC, the inset picture is the plot of pseudo-second-order adsorption model. (b) The intra-particle diffusion rate constants of MB and MO adsorption by MBMC (adsorbent dosage 20 mg/L, initial dye concentrations 150 mg/L, pH 7.0, temperature 25 °C).

possessed by divalent electrolyte ($Ca(NO_3)_2$) than univalent electrolyte (NaCl).

### 3.4. Adsorption kinetics

Adsorption kinetic studies are essential as information about adsorption efficiency and mechanism could be provided through the research. According to Fig. 7a, adsorption of MB and MO is a time-dependent process. Significant and rapid decrease of dye concentration could be observed in the first hour, and the adsorption process slowed down and reached the equilibrium within 2 h. The adsorption data were well described by the pseudo-second-order kinetic model (inset picture in Fig. 7a), with correlation coefficients $R^2 > 0.999$ for both MB and MO adsorption; the rate constant ($k_{ad}$) calculated using this model is listed in Table 3.

Although the adsorption data fitted well with the pseudo-second-order model, the diffusion mechanism could not be identified using this equation [25]. Thus intraparticle diffusion model was used to evaluate the mechanism and predict the rate-controlling steps. The plots of $q_t$ versus $t_{1/2}$ are shown in Fig. 7b. It could be observed that the plots are multi-linear and there are three regions, indicating different stages in adsorption process [26]. The intraparticle diffusion constants of each region could be calculated using Eq. (4), and the results were shown in Table 3. The adsorption rate is in the order of first stage ($k_1$) > second stage ($k_2$) > third stage ($k_3$). Both dyes underwent firstly a sharp-sloped stage representing the external mass transfer (slope $k_1$), during which nearly 90% of dyes were adsorbed onto the external surface of the adsorbent. When the adsorption onto the external surface reached saturation, the second stage began (slope $k_2$), and the dyes entered the pores of the adsorbents and were adsorbed onto the internal surface of the mesopores. With the decrease of dye molecule concentrations, the intraparticle diffusion starts to slow down and reached equilibrium stage (slope $k_3$) [16]. Since the rate of external transfer (slope $k_1$) was higher that of internal transfer (slope $k_2$ and $k_3$), thus the rate limiting step might be internal transfer, and the rate was governed by a particle diffusion [27].

### 3.5. Adsorption isotherm and thermodynamic studies

Adsorption isotherm studies are important for investigating the adsorption behavior and mechanisms. Langmuir and Freundlich isotherms were used to normalize the equilibrium data, with the results summarized in Table 4. From Table 4, it could be demonstrated that Langmuir isotherm fitted better than Freundlich isotherms, with the higher correlation coefficients ($R^2 > 0.980$) under all the temperatures studied. Since Langmuir model assumes monolayer adsorption, the existence of homogenous active sites of the adsorbents could be indicated [28]. And all the values of n were found to be more than 1, while the values of $R_L$ for MB and MO were in the range from 0.261 to 0.855 and from 0.251 to 0.856, respectively, demonstrating that the adsorption process could be considered as favorable [29]. As further reflected from Table 4, the adsorption capacity for both of the two dyes increased with temperature, demonstrating the adsorption processes were endothermic in nature.

**Table 3**
Pseudo-second-order parameters and intraparticle diffusion rates.

| | Pseudo-second-order parameters | Intraparticle diffusion rates | | |
|---|---|---|---|---|
| | $k_{ad}$ ($\times 10^{-3}$ mg g$^{-1}$ min$^{-1}$) | $k_{id,1}$ | $k_{id,2}$ | $k_{id,3}$ (mg g$^{-1}$ h$^{-1/2}$) |
| MB | 0.91 | 276.47 | 68.10 | 0.54 |
| MO | 1.02 | 234.63 | 73.86 | 0.32 |

**Table 4**
Isotherm parameters for the adsorption of MB and MO onto MBMC.

| Dye | $T$ (K) | Langmuir model | | Freundlich model | | | |
|---|---|---|---|---|---|---|---|
| | | $q_m$ (mg/g) | $b$ (L/mg) | $R^2$ | $K_F$ | $n$ | $R^2$ |
| MB | 298 | 959.5 | 0.00339 | 0.983 | 26.5 | 2.01 | 0.934 |
| | 308 | 975.7 | 0.00344 | 0.989 | 27.4 | 2.02 | 0.942 |
| | 318 | 987.5 | 0.00354 | 0.993 | 28.7 | 2.03 | 0.950 |
| MO | 298 | 849.3 | 0.00337 | 0.981 | 23.7 | 2.02 | 0.942 |
| | 308 | 864.1 | 0.00346 | 0.989 | 24.8 | 2.03 | 0.951 |
| | 318 | 875.5 | 0.00374 | 0.994 | 28.2 | 2.09 | 0.954 |

To investigate how the reduction of dyes by Fe/Ni in MBMC involved in dyes removal, we prepared mesoporous carbon (MC) using the same procedure for the synthesis of MBMC except adding small amounts of $HNO_3$ instead of metal nitrates [17], and then compared the removal amounts of MC and MBMC, with the results shown in Fig. S1. As demonstrated in Fig. S1, the removal amounts by MC were slightly higher than MBMC, indicating that the reduction effects by Fe/Ni nanoparticles in MBMC did not play an important role in dye removal compared with the adsorption effects of the mesoporous carbons.

Moreover, it has been reported that in $Fe^0/H_2O$ systems, Methylene blue (MB) was reduced to colorless leukomethylene blue (LMB) [30]. Therefore, if MB was reduced by MBMC, after separating MBMC from the solution, the residual solution would contain both LB and LMB. Since manganese dioxide ($MnO_2$) could oxidize MB, and at the same time re-oxidize LMB to MB [30], the addition of $MnO_2$ into the residual MB solution could result in both the oxidation of MB and LMB. However, in the fresh MB solution containing only MB, $MnO_2$ was only used for oxidizing MB, resulting in the higher oxidized amounts of MB. Thus the oxidized amounts using $MnO_2$ could be used as an index for the information of reduction. MB removal efficiencies using $MnO_2$ are listed in Table S1. Since no obvious difference could be observed between the efficiencies in the fresh and residual solutions, it could be conferred that the reduction effects by Fe/Ni nanoparticles doped mesoporous carbon was not obvious. No obvious reduction using MBMC might be attributed to the low amounts of Fe/Ni nanoparticles, the content of which might be around 10% of the total weight of MBMC [17]. And the adsorption capacity of the mesoporous carbons was really high, thus it might be difficult to distinguish the reduction effects. Even for the bare Fe/Ni alloy, the adsorption effects were dominant in the removal [31]. Moreover, it has been reported that lower ratio of Ni in the Fe/Ni alloy would be more beneficial for the pollutant reduction [31]. Therefore, our future research would be focused on the optimization of the Fe/Ni ratio and Fe/Ni contents in mesoporous carbon.

The thermodynamic parameters could be used to evaluate the orientation and feasibility of adsorption reactions. Table 5 shows the negative values of $\Delta G$, indicating that the adsorption processes were spontaneous. The positive values of $\Delta H$ further confirmed that the adsorption reactions were endothermic. The positive values of $\Delta S$ indicated the affinity of MBMC for the dyes and the increased randomness at the solid–solution interface with some structural changes occurred to the dye molecules and MBMC during the adsorption process [32]. Similar results were also found in the adsorption of malachite green and rhodamine B onto activated carbon [33].

**Table 5**
Thermodynamic parameters for the adsorption of MB and MO by MBMC at different temperatures.

| Dye | Temperature (K) | $\Delta G$ (kJ/mol) | $\Delta H$ (kJ/mol) | $\Delta S$ (kJ/mol) |
|---|---|---|---|---|
| MB | 298 | −17.31 | 1.64 | 0.064 |
| | 308 | −17.92 | | |
| | 318 | −18.58 | | |
| MO | 298 | −17.35 | 4.08 | 0.080 |
| | 308 | −17.94 | | |
| | 318 | −18.73 | | |

### 3.6. Spatial effects of the dyes

It has been reported that the adsorption capacity was also affected by the spatial effects of the dyes, and the investigation of the spatial effects of dyes could help further understand the correlation between the adsorbent and adsorbate [34,35]. As shown in Table 1 and Fig. 1, the five dyes studied here could be divided into three groups according to their molecular structures: one is MB and MO with short chain and smaller molecular size; another one is BY with the long chain and larger molecular size; and the rest one is RB and RR2, which has 3D molecular structure. The equilibrium adsorption capacities of the five dyes in adsorption system containing 500 mg/L of each dye were calculated using Eq. (1) and listed in Table 6. It could be observed in Table 6 that there was no significant difference in the adsorption capacity for BY and the ones for MB and MO, although the molecular size of BY was much larger than those of MB and MO. However, for the adsorption of RB and AA2 with large molecular sizes, the adsorbed amount of them were much lower than that of BY. The phenomenon indicated that the hindrance on MBMC is not distinct with the size of the dye molecules, but the larger adsorption steric hindrance of 3D molecular structure could result in less occupancy of pores and lower adsorption capacity, and similar phenomenon was also reported in dye adsorption by bimodal mesoporous carbon [19]. Therefore, it could be demonstrated that the spatial effect of dye molecules played a significant role in adsorption.

### 3.7. Adsorption in primary and secondary pores

In order to further understand the roles of the primary and secondary pores and the correlation between the adsorbent and adsorbate, $N_2$ adsorption–desorption isotherms were also used to evaluate adsorbents after MB and MO adsorption. As indicated in Fig. 2a, the two hysteresis loops of the isotherm were retained after adsorption, and the pore size distribution (Fig. 2b) also confirmed the presence of bimodal-like mesostructures after adsorption. The surface area, pore volume and most probable size distribution of MBMC after adsorption are also listed in Table 2, and the decrease of both surface area and pore volume after adsorption confirmed the adsorption of dyes into the pores. It could be indicated from the decrease in both of the primary pore and secondary pore size (Fig. 2b and Table 2) after both MB and MO adsorption that dyes were also adsorbed onto both of the primary and the secondary pores. Compared with the adsorbed amount by several different adsorbents in the literatures listed in Table 7, MBMC exhibited higher adsorption capacity than most of the adsorbents reported. And the adsorption capacity of MBMC was higher than the unimodal mesoporous materials reported. It has been reported that the aggregation of large molecules in the orifice of pores with small diameters resulted in the blockage of pores [19], thus the two mesopores, especially the large secondary mesopores could greatly enhance the diffusion and loading of the bulky dye molecules. And

**Table 6**
The equilibrium adsorption capacity ($q_e$) for different dyes on MBMC.

| Dye | MB | MO | BY | RB | RR2 |
|---|---|---|---|---|---|
| $q_e$ (mg/g) | 641.3 | 569.3 | 587.1 | 430.7 | 372.4 |

**Table 7**
Comparison of maximum adsorption capacity ($q_m$) for adsorption of MB and MO by various adsorbents reported in the literature.

| Adsorbent | Adsorbate | Temperature | $q_m$ (mg/g) | References |
|---|---|---|---|---|
| SBA-15 | MB | 25 | 65.79 | [29] |
| Mesoporous carbon from alkaline treated zeolite X | MB | 20 | 436.55 | [36] |
| Iron terephthalate | MB | 25 | 187 | [37] |
| Rice husk | MB | 32 | 40.59 | [38] |
| Alkali-activated multiwalled carbon Nanotubes | MB | 25 | 399 | [39] |
| MBMC | MB | 25 | 959.5 | This study |
| CMK-3 | MO | 25 | 294.1 | [40] |
| Phragmites australis activated carbon | MO | 30 | 217.4 | [36] |
| Iron terephthalate | MO | 25 | 477 | [41] |
| Alkali-activated multiwalled carbon nanotubes | MO | 25 | 149 | [39] |
| Magnetic chitosan beads | MO | 20 | 779 | [41] |
| MBMC | MO | 25 | 849.3 | This study |

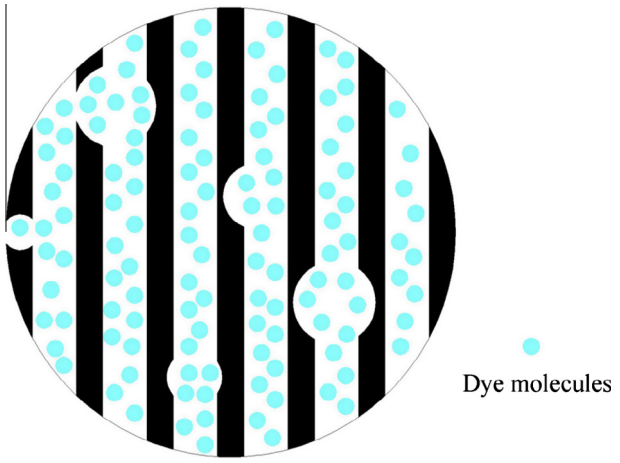


**Fig. 8.** Schematic diagram for dye adsorption using MBMC with bimodal pore systems.

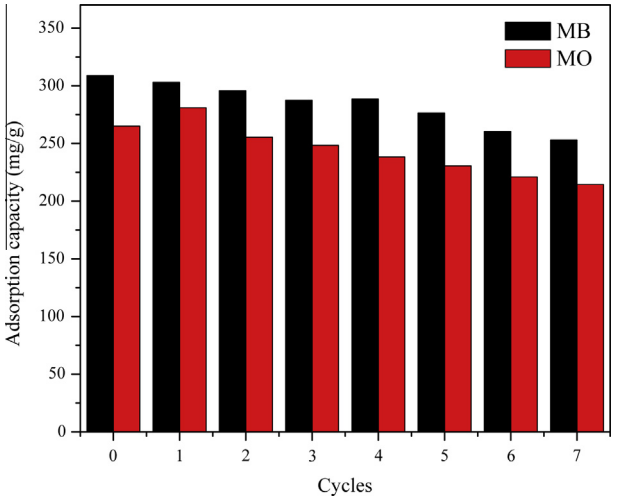


**Fig. 9.** Adsorption capacity of MBMC for MB and MO for seven consecutive adsorption–desorption cycles.

the schematic diagram for dye adsorption in the primary and secondary mesopores is illustrated in Fig. 8.

### 3.8. Adsorbent regeneration

After adsorption, MBMC was regenerated by washing the samples using ethanol. Fig. 9 shows the adsorption performance of the regenerated MBMC for MB and MC. Although the adsorption capacity for both MB and MO decreased gradually with the increasing desorption cycles, the regenerated MBMC still exhibited good performance for MB and MO adsorption. After desorption for the seventh cycle, the adsorbed amounts of MB and MO by MBMC were 253.1 mg/g and 214.5 mg/g, which was almost 82% and 81% of the adsorption capacity by the fresh material, respectively. Thus it could be indicated that the adsorbent could be regenerated and reused effectively.

## 4. Conclusions

In this study, highly effective adsorption of cationic dye MB and anionic dye MO has been demonstrated on Fe/Ni nanoparticles doped bimodal mesoporous carbon. The physicochemical analysis data has demonstrated bimodal-like pore size distribution and good magnetic performance of MBMC. Alkaline conditions were favorable for MB adsorption, while acidic conditions were better for MO adsorption. And higher adsorption capacity could be reached when the ionic concentration increased. Adsorption onto MBMC was also affected by the molecular structures of different dyes, and both primary and secondary pores were involved in dye adsorption. Adsorption equilibrium could be reached within 2 h, and the adsorption kinetics was well described by the pseudo-second-order kinetic model. The diffusion mechanism indicated that adsorption of both MB and MO exhibited 3-stage process. Langmuir model was most appropriate to fit the adsorption data, and the estimated maximum adsorption capacity for MB (959.5 mg/g) and MO (849.3 mg/g) was higher than the unimodal mesoporous carbon and most of other materials reported. Thermodynamic studies indicated that the adsorption was a spontaneous, endothermic process. Moreover, MBMC could be regenerated and reused using ethanol. The results indicate that MBMC shows potential application for cationic and anionic dye removal in industrial effluents.

## Acknowledgments

The study was financially supported by the Young Top-Notch Talent Support Program of China (2012), the National Natural Science Foundation of China (51378190 and 51222805), the Program for New Century Excellent Talents in University from the Ministry of Education of China (NCET-11-0129), Interdisciplinary Research Project of Hunan University, the Fundamental Research Funds for the Central Universities, Hunan University and the Program for Changjiang Scholars and Innovative Research Team in University (IRT-13R17), Hunan University and the Hunan Provincial Innovation Foundation For Postgraduate (CX2009B080).

## Appendix A. Supplementary material

Supplementary data associated with this article can be found, in the online version, at http://dx.doi.org/10.1016/j.jcis.2015.02.037.

## References

[1] W.-W. Tang, G.-M. Zeng, J.-L. Gong, J. Liang, P. Xu, C. Zhang, B.-B. Huang, Sci. Total Environ. 468–469 (2014) 1014–1027.
[2] Zeng Guangming, Chen Ming, Z. Zhuotong, Science 340 (2013) 1403.

[3] J.-L. Gong, B. Wang, G.-M. Zeng, C.-P. Yang, C.-G. Niu, Q.-Y. Niu, W.-J. Zhou, Y. Liang, J. Hazard. Mater. 164 (2009) 1517–1522.
[4] Guangming Zeng, Ming Chen, Z. Zeng, Nature 499 (2013) 154.
[5] L. Tang, Y. Cai, G. Yang, Y. Liu, G. Zeng, Y. Zhou, S. Li, J. Wang, S. Zhang, Y. Fang, Y. He, Appl. Surf. Sci. 314 (2014) 746–753.
[6] C. He, X. Hu, Ind. Eng. Chem. Res. 50 (2011) 14070–14083.
[7] P. Xu, G.M. Zeng, D.L. Huang, C.L. Feng, S. Hu, M.H. Zhao, C. Lai, Z. Wei, C. Huang, G.X. Xie, Z.F. Liu, Sci. Total Environ. 424 (2012) 1–10.
[8] A.K. Sinha, M. Pradhan, S. Sarkar, T. Pal, Environ. Sci. Technol. 47 (2013) 2339–2345.
[9] G. Zeng, Y. Liu, L. Tang, G. Yang, Y. Pang, Y. Zhang, Y. Zhou, Z. Li, M. Li, M. Lai, X. He, Y. He, Chem. Eng. J. 259 (2015) 153–160.
[10] Y. Pang, G. Zeng, L. Tang, Y. Zhang, Y. Liu, X. Lei, Z. Li, J. Zhang, Z. Liu, Y. Xiong, Chem. Eng. J. 175 (2011) 222–227.
[11] C. Liang, Z. Li, S. Dai, Angew. Chem. Int. Ed. 47 (2008) 3696–3717.
[12] L. Tang, G.-D. Yang, G.-M. Zeng, Y. Cai, S.-S. Li, Y.-Y. Zhou, Y. Pang, Y.-Y. Liu, Y. Zhang, B. Luna, Chem. Eng. J. 239 (2014) 114–122.
[13] Y. Zhou, L. Tang, G. Zeng, J. Chen, Y. Cai, Y. Zhang, G. Yang, Y. Liu, C. Zhang, W. Tang, Biosens. Bioelectron. 61 (2014) 519–525.
[14] Y. Zhang, G.-M. Zeng, L. Tang, D.-L. Huang, X.-Y. Jiang, Y.-N. Chen, Biosens. Bioelectron. 22 (2007) 2121–2126.
[15] Y. Liu, Z. Zeng, G. Zeng, L. Tang, Y. Pang, Z. Li, C. Liu, X. Lei, M. Wu, P. Ren, Z. Liu, M. Chen, G. Xie, Bioresour. Technol. 115 (2012) 21–26.
[16] G. Li, Z. Zhao, J. Liu, G. Jiang, J. Hazard. Mater. 192 (2011) 277–283.
[17] Z. Wang, X. Liu, M. Lv, J. Meng, Carbon 48 (2010) 3182–3189.
[18] Y. Wang, M. Yao, Y. Chen, Y. Zuo, X. Zhang, L. Cui, J. Alloys Compd. 627 (2014) 7–12.
[19] X. Zhuang, Y. Wan, C. Feng, Y. Shen, D. Zhao, Chem. Mater. 21 (2009) 706–716.
[20] D. Zhao, Q. Huo, J. Feng, B.F. Chmelka, G.D. Stucky, J. Am. Chem. Soc. 120 (1998) 6024–6036.
[21] M. Sevilla, P. Valle-Vigón, P. Tartaj, A.B. Fuertes, Carbon 47 (2009) 2519–2527.
[22] P.T. Tanev, L.T. Vlaev, J. Colloid Interface Sci. 160 (1993) 110–116.
[23] W. Konicki, D. Sibera, E. Mijowska, Z. Lendzion-Bieluń, U. Narkiewicz, J. Colloid Interface Sci. 398 (2013) 152–160.
[24] S.A. Ahmed, E.M. Soliman, Appl. Surf. Sci. 284 (2013) 23–32.
[25] M. Doğan, H. Abak, M. Alkan, J. Hazard. Mater. 164 (2009) 172–181.
[26] N.V. Perez-Aguilar, P.E. Diaz-Flores, J.R. Rangel-Mendez, J. Colloid Interface Sci. 364 (2011) 279–287.
[27] M.P. Tavlieva, S.D. Genieva, V.G. Georgieva, L.T. Vlaev, J. Colloid Interface Sci. 409 (2013) 112–122.
[28] S.J. Gragg, K.S.W. Sing, Adsorption, Surface Area and Porosity, second ed., Academic Press, London, 1982. pp. 4–287.
[29] C.-H. Huang, K.-P. Chang, H.-D. Ou, Y.-C. Chiang, C.-F. Wang, Micropor. Mesopor. Mater. 141 (2011) 102–109.
[30] C. Noubactep, J. Hazard. Mater. 166 (2009) 79–87.
[31] C. Lin, Y. Shih, J. MacFarlane, Chem. Eng. J. 262 (2015) 59–67.
[32] H. Javadian, P. Vahedian, M. Toosi, Appl. Surf. Sci. 284 (2013) 13–22.
[33] L. Wang, J. Zhang, R. Zhao, C. Li, Y. Li, C. Zhang, Desalination 254 (2010) 68–74.
[34] S.R. Sandeman, V.M. Gun'ko, O.M. Bakalinska, C.A. Howell, Y. Zheng, M.T. Kartel, G.J. Phillips, S.V. Mikhalovsky, J. Colloid Interface Sci. 358 (2011) 582–592.
[35] A.M. Donia, A.A. Atia, W.A. Al-amrani, A.M. El-Nahas, J. Hazard. Mater. 161 (2009) 1544–1550.
[36] C. Yan, C. Wang, J. Yao, L. Zhang, X. Liu, Colloids Surf. A 333 (2009) 115–119.
[37] E. Haque, J.W. Jun, S.H. Jhung, J. Hazard. Mater. 185 (2011) 507–511.
[38] V. Vadivelan, K.V. Kumar, J. Colloid Interface Sci. 286 (2005) 90–100.
[39] J. Ma, F. Yu, L. Zhou, L. Jin, M. Yang, J. Luan, Y. Tang, H. Fan, Z. Yuan, J. Chen, ACS Appl. Mater. Interfaces 4 (2012) 5749–5760.
[40] N. Mohammadi, H. Khani, V.K. Gupta, E. Amereh, S. Agarwal, J. Colloid Interface Sci. 362 (2011) 457–462.
[41] S. Chen, J. Zhang, C. Zhang, Q. Yue, Y. Li, C. Li, Desalination 252 (2010) 149–156.